THE JOURNAL OF BIOLOGICAL CHEMISTRY
Vol. 279, No. 3, Issue of January 16, pp. 2242–2253, 2004

Printed in U.S.A.

The Crystal Structures of *Klebsiella pneumoniae* Acetolactate Synthase with Enzyme-bound Cofactor and with an Unusual Intermediate*

Received for publication, April 17, 2003, and in revised form, October 10, 2003
Published, JBC Papers in Press, October 13, 2003, DOI 10.1074/jbc.M304038200

Siew Siew Pang‡, Ronald G. Duggleby‡§, Richard L. Schowen¶, and Luke W. Guddat‡

From the ‡Department of Biochemistry and Molecular Biology, the University of Queensland, Brisbane, Queensland 4072, Australia and the ¶Department of Chemistry, the University of Kansas, Lawrence, Kansas 66045

Acetohydroxyacid synthase (AHAS) and acetolactate synthase (ALS) are thiamine diphosphate (ThDP)-dependent enzymes that catalyze the decarboxylation of pyruvate to give a cofactor-bound hydroxyethyl group, which is transferred to a second molecule of pyruvate to give 2-acetolactate. AHAS is found in plants, fungi, and bacteria, is involved in the biosynthesis of the branched-chain amino acids, and contains non-catalytic FAD. ALS is found only in some bacteria, is a catabolic enzyme required for the butanediol fermentation, and does not contain FAD. Here we report the 2.3-Å crystal structure of *Klebsiella pneumoniae* ALS. The overall structure is similar to AHAS except for a groove that accommodates FAD in AHAS, which is filled with amino acid side chains in ALS. The ThDP cofactor has an unusual conformation that is unprecedented among the 26 known three-dimensional structures of nine ThDP-dependent enzymes, including AHAS. This conformation suggests a novel mechanism for ALS. A second structure, at 2.0 Å, is described in which the enzyme is trapped halfway through the catalytic cycle so that it contains the hydroxyethyl intermediate bound to ThDP. The cofactor has a tricyclic structure that has not been observed previously in any ThDP-dependent enzyme, although similar structures are well known for free thiamine. This structure is consistent with our proposed mechanism and probably results from an intramolecular proton transfer within a tricyclic carbanion that is the true reaction intermediate. Modeling of the second molecule of pyruvate into the active site of the enzyme with the bound intermediate is consistent with the stereochemistry and specificity of ALS.

The enzyme EC 2.2.1.6 (formerly EC 4.1.3.18) known both as acetolactate synthase (ALS)[1] and as acetohydroxyacid synthase (AHAS) catalyzes the conversion of 2 mol of pyruvate to acetolactate plus CO_2 (1). These two different names for the enzyme distinguish two forms (2) that have distinctly different properties. One difference is that AHAS requires FAD, whereas ALS is FAD-independent. However, ALS and AHAS are clearly related proteins with substantial sequence similarities and share a requirement for thiamine diphosphate (ThDP).

In most flavin-containing enzymes that catalyze non-redox reactions (3), the cofactor has been shown, or is suspected, to play an internal role as an electron acceptor/donor. For example, in chorismate synthase, flavin mononucleotide participates in free radical chemistry (4). The exception is hydroxynitrile lyase, where there appears to be no internal redox role (5). In a curious parallel to ALS/AHAS, this enzyme exists in two forms, only one of which contains FAD (6).

The three-dimensional structure of the FAD-dependent almond hydroxynitrile lyase (7) suggests that the cofactor is an evolutionary remnant of an aryl alcohol oxidase progenitor. Similarly, AHAS may have evolved from a pyruvate oxidase ancestor (8). Our determination of the structure of the FAD-dependent yeast AHAS (9) supports this idea; FAD is located close to the active site and in a position similar to that in pyruvate oxidase. The function of FAD in AHAS appears to be solely for maintenance of structural integrity.

An alternative approach to unraveling the role of FAD in AHAS is to understand how the FAD-independent ALS can dispense with this cofactor. This enzyme, from *Aerobacter aerogenes*, was crystallized in 1967 (10), but no x-ray diffraction studies were reported. We obtained diffraction-quality crystals of the enzyme from the closely related bacterium *Klebsiella pneumoniae* (11); now we report the three-dimensional structure of this ALS.

ThDP-dependent enzymes are ubiquitous in nature and are involved in all major metabolic processes. It is generally accepted that the initial step in catalysis by these enzymes is the deprotonation of the thiazolium ring at the C-2 atom (Fig. 1, *A*, ***I*** → ***II***, and *B*). Elucidation of the structure of several ThDP-dependent enzymes (12–18) has allowed a plausible mechanism for this ionization to be proposed, involving a conserved glutamate, N-1′, and the 4′-amino group. Studies with cofactor analogs (19) and by mutagenesis (20–24) support this mechanism.

The high specific activity of *K. pneumoniae* ALS (10) corresponds to a k_{cat} of 533 s^{-1} which is about 10-fold higher than that of any FAD-dependent AHAS (*e.g.* Ref. 25) showing that FAD independence does not cripple the enzyme. Quite the reverse; the FAD-dependent enzyme is unable to achieve rate enhancements that are attainable by ALS. The k_{cat} value of *K. pneumoniae* ALS is significantly higher than that of any ThDP-dependent enzyme with a known structure. The k_{cat} value is also substantially higher than the observed rate constant for C-2 deprotonation in *Zymomonas mobilis* pyruvate decarboxylase and in yeast transketolase (26), suggesting that the environment of ThDP in *K. pneumoniae* ALS might be especially favorable for C-2 deprotonation.

* This work was supported by Grant A00105313 (to R. G. D. and L. W. G.) by the Australian Research Council. The costs of publication of this article were defrayed in part by the payment of page charges. This article must therefore be hereby marked "*advertisement*" in accordance with 18 U.S.C. Section 1734 solely to indicate this fact.

§ To whom correspondence should be addressed. Tel.: 61-7-3365-4615; Fax: 61-7-3365-4699; E-mail: Ronald.Duggleby@mailbox.uq.edu.au.

[1] The abbreviations used are: ALS, acetolactate synthase; AHAS, acetohydroxyacid synthase; DTT, dithiothreitol; r.m.s.d., root mean square deviation; ThDP, thiamine diphosphate.

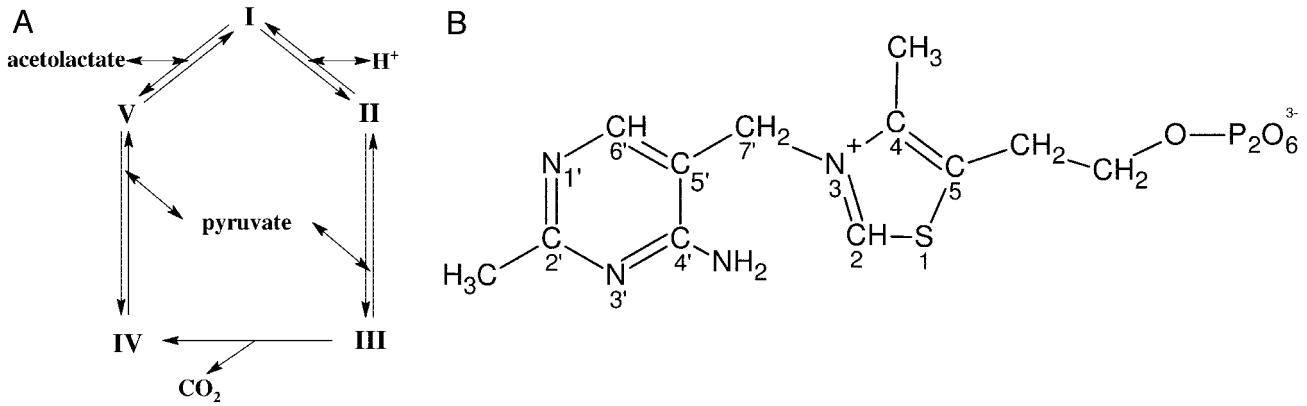

FIG. 1. **The catalytic cycle of ALS and AHAS.** The accepted view (*A*) is that enzyme-bound ThDP (***I***) ionizes to give the carbanion (***II***) that then reacts with pyruvate to give lactyl-ThDP (***III***). After decarboxylation, the intermediate formed (***IV***) reacts with a second molecule of pyruvate to give acetolactyl-ThDP (***V***). Release of acetolactate completes the catalytic cycle. *B* shows the structure of ThDP.

Here we report, at 2.3-Å resolution, the structure of the enzyme containing ThDP and the other essential cofactor Mg^{2+}; henceforth, this complex will be denoted the "resting" enzyme. ThDP is bound in a conformation that is slightly, but significantly, different from that found in all other ThDP-dependent enzymes. We propose a mechanism for C-2 deprotonation that implies an active role for the sulfur atom of ThDP, similar to a suggestion by Kluger (27).

Only two of the reported structures of ThDP-dependent enzymes have intermediates attached to the cofactor. These are pyruvate:ferredoxin oxidoreductase (28) containing the acetyl radical of ThDP (formed from pyruvate) and transketolase (29) with the α-carbanion or enamine of dihydroxyethyl-ThDP (formed from hydroxypyruvate). For both enzymes, trapping of the intermediate results because no acceptor substrate is present to complete the catalytic cycle. For 2-ketoacid decarboxylases such as pyruvate decarboxylase, there is no second substrate, so intermediate capture does not seem to be feasible. Superficially, the same is true for ALS/AHAS; although there is a second substrate, it cannot be omitted because it is chemically identical to the first substrate. However, we realized that the catalytic cycle of ALS/AHAS possesses an unusual feature that makes intermediate capture inevitable, as we shall show later. The second structure reported here, at both 2.0- and 2.3-Å resolution, is of *K. pneumoniae* ALS containing the intermediate formed after decarboxylation of the first pyruvate. The intermediate formed appears to be the hydroxyethyl derivative of the tricyclic form of ThDP.

MATERIALS AND METHODS

Expression and purification of *K. pneumoniae* ALS were as described previously (11). Prior to crystallization, the enzyme was concentrated to 9 mg/ml in 50 mM potassium phosphate buffer (pH 7.0) containing 1 mM ThDP, 1 mM $MgCl_2$, and 1 mM DTT. Crystals of the enzyme grown in hanging drops (1 μl of reservoir solution and 1 μl of protein solution) and incubated at 17 °C appeared overnight and reached their maximum size in 2 weeks. The reservoir solution consisted of 0.1 M Na-Hepes (pH 7.5–7.7), 6–8% (w/v) PEG8000, and 6–9% (v/v) ethylene glycol. The crystals reported previously (11) belong to the space group *C*2, and diffract to 2.6-Å resolution, but in subsequent crystallization experiments using the same conditions, orthorhombic and triclinic crystals were obtained (Table I). Because the *C*2 crystals diffract to moderate resolution only, further structural studies were pursued with the new crystal forms. To trap the intermediate, orthorhombic and triclinic crystals were soaked in 200 mM pyruvate (K_m = 34.1 ± 3.9 mM) for 1 week. For cryoprotection, crystals were transferred to 5 μl of reservoir solution containing 30% (v/v) PEG600.

For this study, three complete data sets were collected; one of the resting enzyme (*i.e.* without added pyruvate) and two of the enzyme-intermediate complex formed by soaking with pyruvate. An orthorhombic crystal was used to collect data on the resting enzyme, and data from an orthorhombic and a triclinic crystal were collected for the enzyme-intermediate complex. The three data sets were collected on Beam-Line 14D at the Advanced Photon Source in the Argonne National Laboratory, Chicago. The data were indexed, integrated, and scaled using the programs DENZO and SCALEPACK (30).

The structures of the enzyme-intermediate complex, in the orthorhombic and triclinic crystals, were solved concurrently using AMoRe (31). The search molecule for both forms was a dimer of the core region (residues 94–256, 289–383, 403–438, and 491–646) of the catalytic subunit of yeast AHAS (PDB code 1JSC, see Ref. 9). By using the AHAS dimer as the probe, two peaks in the rotation function were observed, both of which had correlation coefficients of 0.257. This compared with a correlation coefficient of 0.067 for the next highest peak. The translation function positioning the second dimer relative to the first was next calculated. The highest peak resulted in assembly of the expected tetramer. The correlation coefficient for this solution was 0.448. Rigid body refinement of the model, using data from 15 to 4 Å, gave an R_{factor} of 0.424. For the orthorhombic crystal, a dimer in the asymmetric unit was observed in the rotation and translation function calculations. The solution had a correlation coefficient of 0.290 and an R_{factor} of 0.550. Rigid body refinement of the model, using data from 15 to 4 Å, gave a correlation coefficient of 0.560 and an R_{factor} of 0.437. The structure of the resting enzyme was determined using the coordinates of the orthorhombic enzyme-intermediate complex as a starting point. Model building and refinement of the three structures were carried out using the program O (32) and the CNS software package (33). The final values for R_{free} and R_{factor} and the errors in the model geometry for the three structures are listed in Table I. The coordinates and structure factors have been deposited with the RCSB Protein Data Bank with PDB codes 1OZF (orthorhombic resting enzyme), 1OZG (orthorhombic + pyruvate), and 1OZH (triclinic + pyruvate). Figures were generated with SETOR (34), MOLSCRIPT (35), Raster3D (36), ChemSketch (Advanced Chemistry Development Inc., Toronto, Canada), ESPript (37) and INSIGHT2000.1 (Accelrys).

RESULTS

Resting Enzyme

Overall Structure of the Resting Enzyme—K. pneumoniae ALS is composed of 559-residue subunits (38), thought to be arranged as a homotetramer as in its *A. aerogenes* counterpart (39). The recombinant ALS that we have crystallized possesses a native N-terminal sequence but has seven additional C-terminal residues, glutamate followed by a hexahistidine sequence. The asymmetric unit in the resting enzyme consists of a dimer, with the other half of the tetramer related by a crystallographic 2-fold axis of symmetry (Fig. 2*A*). Electron density for one subunit (arbitrarily designated monomer A) extends from Val^{7}–His^{554}, except that there is a three-residue gap from Ser^{184}–Ala^{186} in a linker between two domains. No side-chain electron density beyond the β-carbon atom was visible for three polar surface residues Gln^{188}, Lys^{208}, and Lys^{225}. Electron density for monomer B extends by two additional residues at the N terminus but has three gaps: at Val^{118}–Gln^{120} (surface loop), at Ser^{184}–Ala^{186} (domain linker), and at Arg^{362}–

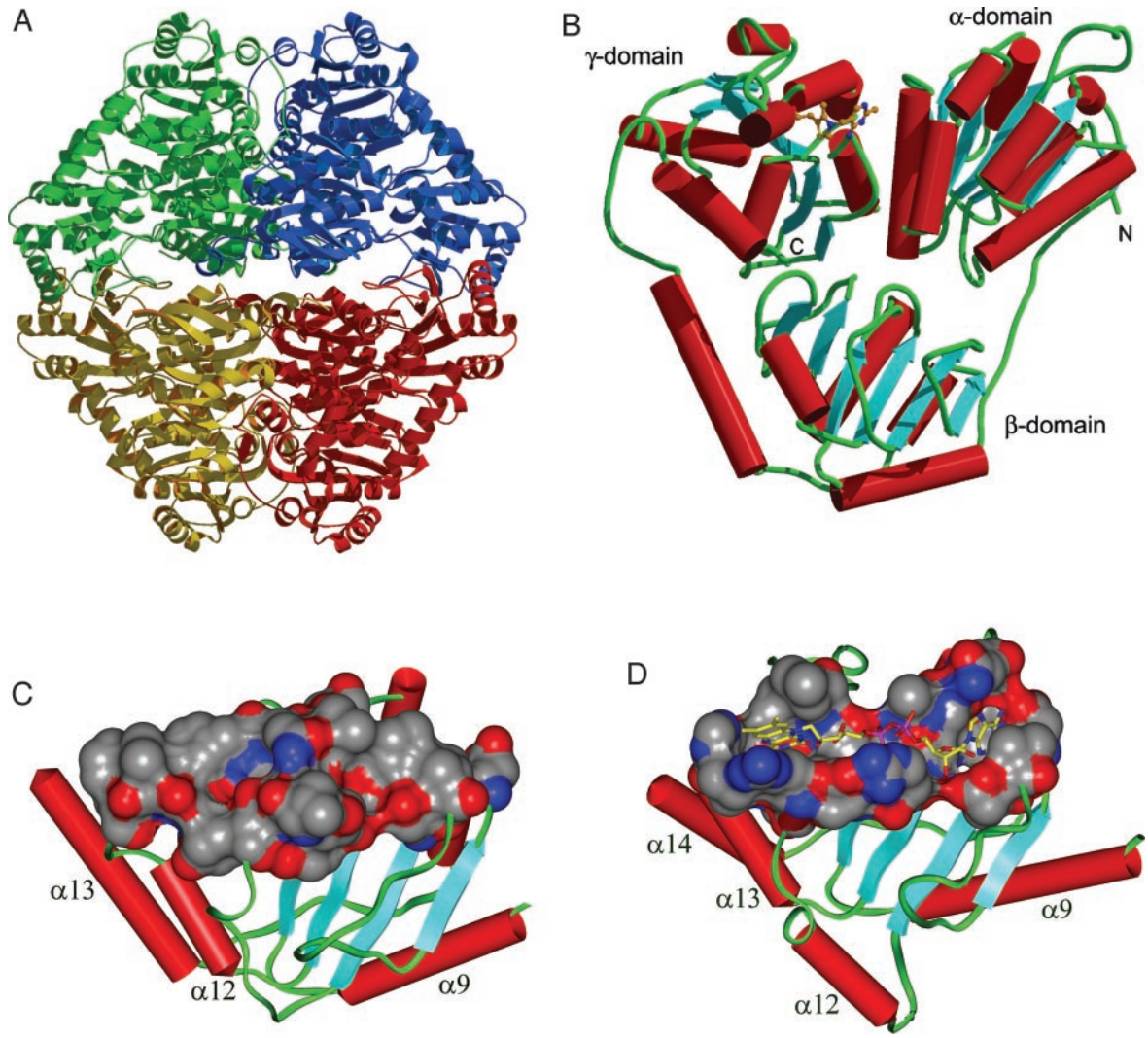

FIG. 2. **Structure of *K. pneumoniae* ALS.** *A* shows a ribbon diagram of the overall structure of the resting enzyme tetramer, with the monomers colored *green* (monomer A), *red* (*B*), *blue* (*C*), and *yellow* (*D*). There is a vertical 2-fold axis of symmetry in this view. The asymmetric unit contains monomers A and B, whereas the active sites are at the AC and BD interfaces. Monomer A is shown in *B*, with cylinder representations of α-helices (*red*) and β-strands (*turquoise*) shown as *arrows*, connected by random coil (*green*). *C* and *D* compare the β-domains of ALS (*C*) and AHAS (*D*), with secondary structure indicated as in *B*. The residues in contact with FAD (*stick model*, *D*) in AHAS and their structural equivalents in ALS (*C*) are shown in surface representation.

Gly^{363} (domain boundary). In monomer B, no side-chain electron density beyond the β-carbon atom was visible for seven polar surface residues Gln^{117}, Gln^{188}, Arg^{228}, Glu^{289}, Arg^{312}, Arg^{350}, and Arg^{361}.

Each monomer is composed of three distinct domains (Fig. 2*B*), designated from the N terminus as the α-, β-, and γ-domains. The α-domain extends from the observable N terminus to Ala^{183}; the β-domain spans residues Pro^{193}–Ser^{342}, and the γ-domain commences at Asp^{360} and extends to the observable C terminus. The connector between the α- and β-domains is a 9-residue random coil, partly undefined in both monomers. The connector between the β- and γ-domains is a well defined 17-residue α-helix, Pro^{343}–Leu^{359} (Fig. 3, *α13*). The α- and γ-domains are each built around a six-stranded parallel β-sheet with the same Richardson topology of $+1x$, $-2x$, $-1x$, $-2x$, $+1x$, surrounded by α-helices. The α-domain has an additional short anti-parallel β-sheet (Fig. 3, *β1/β8*) derived from the N- and C-terminal sections of the domain. The β-domain has a six-stranded parallel β-sheet with a Richardson topology of $+1x$, $+1x$, $-3x$, $-1x$, $-1x$. This β-sheet forms part of a double Rossmann fold. The two monomers are very similar and when overlaid yield a root mean square deviation (r.m.s.d.) of 0.68 Å for 536 equivalent Cα atoms. The most prominent difference is in a small loop that precedes the Val^{118}–Gln^{120} gap in monomer B. The remaining differences are in the β-domain, which is shifted slightly relative to the remainder of the protein.

All ThDP-dependent enzymes have this cofactor bound at the active site in a domain interface, and in most cases the domains are derived from different subunits. The same is true of ALS; however, the crystallographic subunit pair does not correspond to the pair that forms the active site (Fig. 2*A*). Two identical active sites are formed at the interface between monomer A and its symmetry partner. Similarly, monomer B and its symmetry partner form a second pair of identical active sites. Thus, the two functional dimers are each symmetrical but slightly different from one another. These differences most likely originate from crystal packing forces.

Comparison with the FAD-dependent AHAS—The primary and secondary structures of ALS are very similar to those of the FAD-dependent AHAS (Fig. 3). The three-dimensional structures are also very similar. When the α-domains are overlaid (r.m.s.d. = 1.23 Å for 168 Cα atoms), the only noticeable difference is in a loop comprising residues Ala^{112}–Asp^{123}, which adopts a different conformation in the two proteins. This region

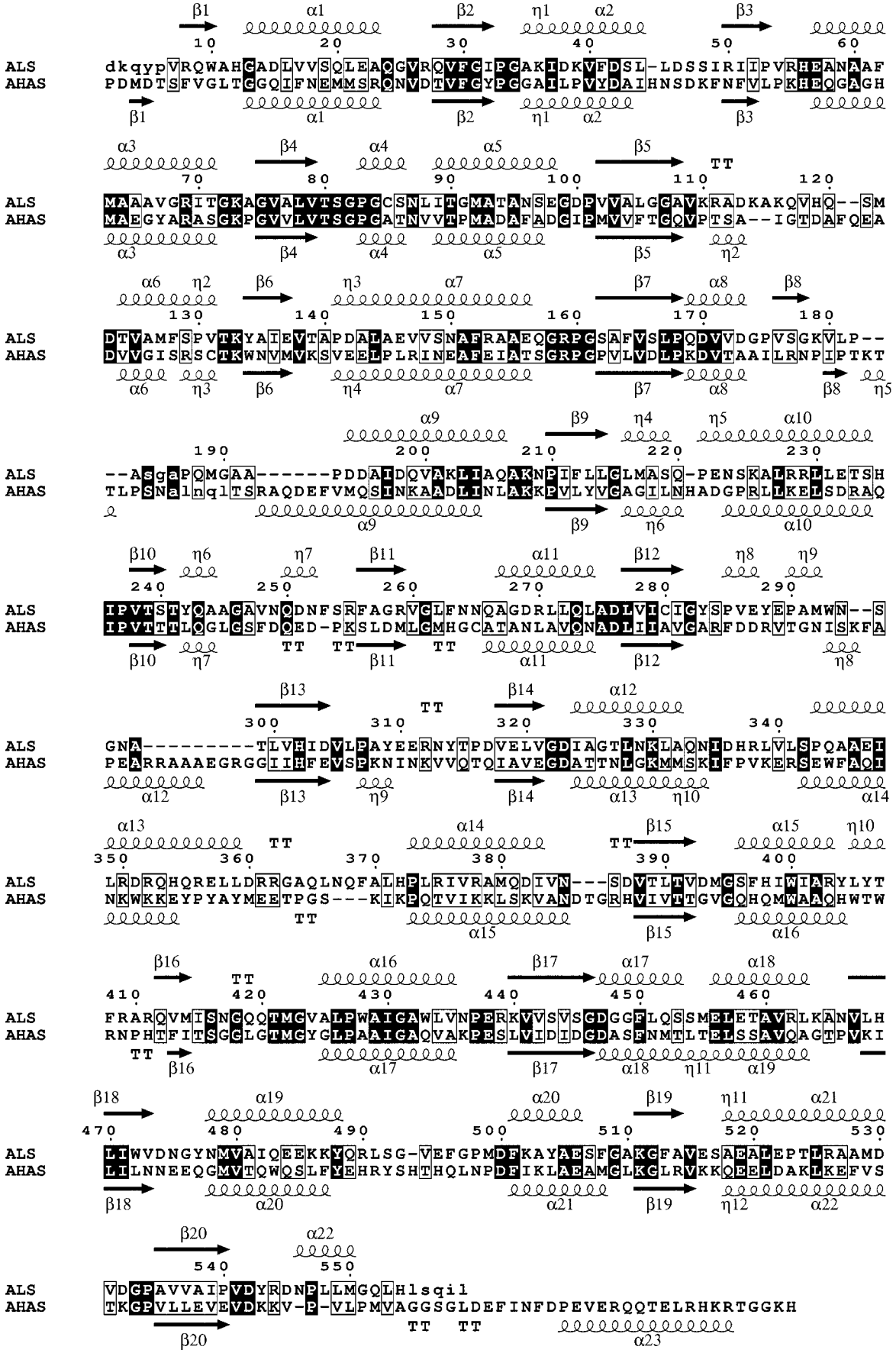

FIG. 3. **Structure-based sequence alignment of *K. pneumoniae* ALS (resting enzyme, monomer A) and yeast AHAS (monomer A, 40), drawn with the program ESPript (37).** The schematics *above* and *below* the sequences represent α-helices (α1, α2, etc.), β-strands (β1, β2, etc.) and 3_{10} helices (η1, η2, etc.), and *TT* represents β-turns. Residues shown in *boxes* are similar between the two sequences, those printed *white* on *black* are identical, and those shown in *lowercase* are not visible in the electron density map of the proteins.

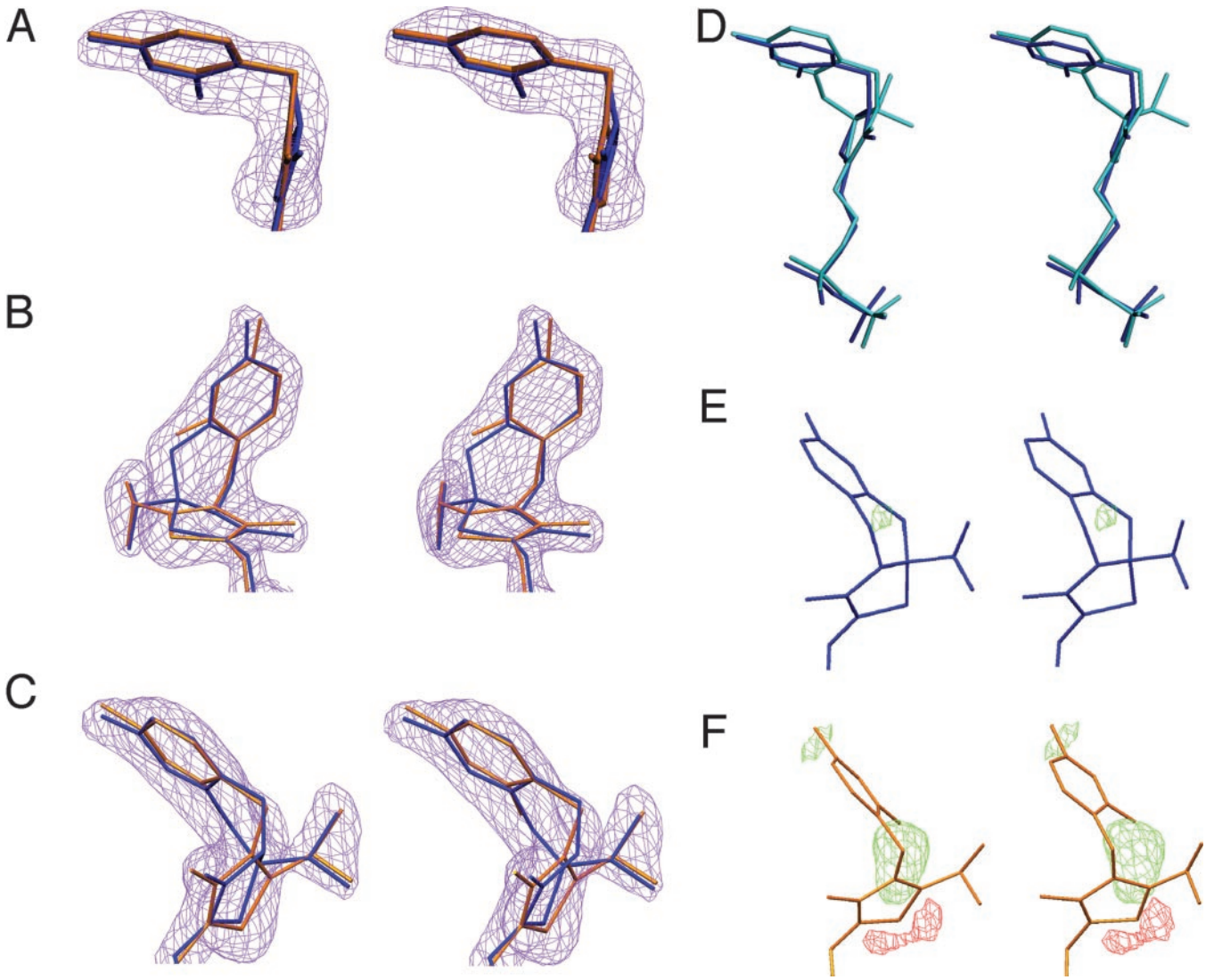

FIG. 4. **Structures and stereo electron density maps for ThDP in *K. pneumoniae* ALS.** *A* shows the $F_o - F_c$ difference electron density map (contoured at $>5\sigma$) for the resting enzyme before ThDP is modeled. The coordinates with a planar N-3 (*brown*) and pyramidal N-3 (*blue*) are overlaid for comparison. *B* and *C* show two views of the $F_o - F_c$ difference electron density map before hydroxyethyl-ThDP was modeled (contoured at $>5\sigma$) for the enzyme intermediate. The coordinates of the modeled tricyclic structure are shown in *blue* and the non-tricyclic model in *brown*. *D*, the coordinates of ThDP with a pyramidal N-3 (*dark blue*) and the tricyclic intermediate (*light blue*) are overlaid. *E* and *F* show the $F_o - F_c$ electron density after modeling of the tricyclic (*E*) and non-tricyclic (*F*) enzyme-intermediate with a C-2 to N-4′ distance of 2.5 Å. *Green* density is contoured at $>3\sigma$ and *red* density at $< -3\sigma$.

in ALS is located at the dimer-dimer interface of the tetramer. Yeast AHAS, on the other hand, does not form a homotetramer and exists as a dimer in both solution and crystals. The γ-domains are also very similar between ALS and AHAS (r.m.s.d. = 1.44 Å for 166 Cα atoms). However, AHAS has a C-terminal extension as described previously (40) that is not found in ALS (Fig. 3).

The β-domains of the two proteins are the most different of the three domains, with a higher r.m.s.d. value (1.49 Å) for fewer (133) Cα atoms. In general, this domain in both enzymes has a similar secondary structure topology, consisting of a central six-stranded parallel β-sheet surrounded by helices and loops. The major differences are in the connections between the strands of the central β-sheet. An example is the polypeptide segment connecting the β-strands 12 and 13 (Fig. 3). In yeast AHAS this segment, comprising residues Gly^{374} to Gly^{401}, consists of two helices that are separated by a random coil. The corresponding region in ALS (Gly^{282}–Ala^{298}) is 11 residues shorter and has two short helices, but neither corresponds to those found in AHAS.

The most obvious difference between the structures of ALS and AHAS is that the latter contains FAD. In AHAS, the FAD-binding site is located mainly in the β-domain. FAD binds near the C-terminal edge of the central parallel β-sheet and forms multiple interactions with a series of loop regions found on the surface of the domain. Most of the interacting amino acid residues are highly conserved among AHAS sequences across plant and fungal and bacterial species. The surface topology of the binding site shows clearly that FAD, in an extended conformation, lies in a groove that runs across the β-domain (Fig. 2*D*). This groove structure is missing from the surface topology of the corresponding area in the β-domain of ALS (Fig. 2*C*). The absence of the groove structure in ALS is brought about by slightly different orientations of the surface loop regions, and by amino acid substitutions to bulky hydrophobic residues at positions that interact with FAD in AHAS.

Structure of ThDP in the Resting Enzyme—ThDP is bound at a subunit interface, anchored at one end through a magnesium ion that is octahedrally coordinated to six oxygen atoms: one from each phosphate group, one from the side chains of Asp^{447}

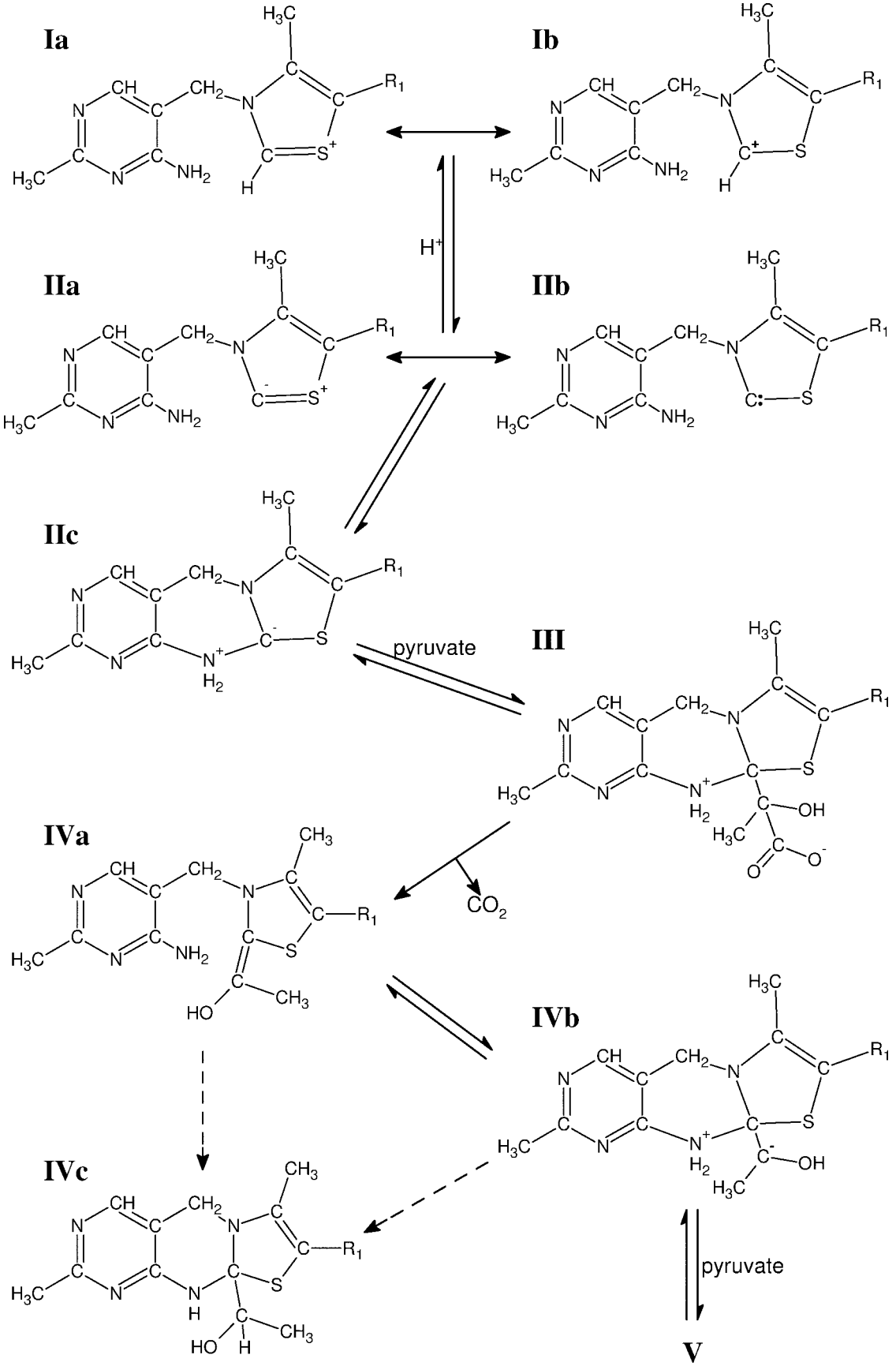

FIG. 5. **Proposed structures in the catalytic cycle of *K. pneumoniae* ALS.** See text for details. ***I–V*** correspond to those in Fig. 1*A*.

and of Asp[474], the backbone of Gly[476], and one water molecule. The arrangement of ligands is slightly unusual compared with other ThDP-dependent enzymes in that the amino acid side-chain ligands are usually an aspartate and an asparagine, which are found at the two ends of the "thiamine-binding motif" discovered by Hawkins *et al.* (41). The asparagine is

highly conserved (42) with the possible exception of ALS sequences. In *Z. mobilis* pyruvate decarboxylase, mutation of the equivalent asparagine to aspartate results in a drastic reduction in the affinity for ThDP (43). The reason that ALS uses aspartate rather than asparagine as a magnesium ion ligand is therefore not clear. What is clear is that the presence of both ThDP and magnesium ion lays to rest the suggestion (38) that *K. pneumoniae* ALS does not require these cofactors.

The first step in catalysis by ThDP-dependent enzymes is widely believed to be the ionization of the thiazolium ring of ThDP (Fig. 1*A*, ***I*** → ***II***). In both ThDP (Fig. 1*B*) and the resulting C-2 carbanions, the thiazolium ring is expected to be planar with its aromaticity producing C-2—N-3 and C-4—C-5 bonds with lengths approaching those of double bonds. This expectation is confirmed in the structures of all ThDP-dependent enzymes containing unmodified ThDP. The bond from N-3 to C-7′, which connects to the methylaminopyrimidine ring, is normally in the same plane as the thiazolium ring due to sp^2 hybridization at N-3. This geometry is observed in the structures of all ThDP-dependent enzymes containing unmodified ThDP. In *K. pneumoniae* ALS the thiazolium ring is planar, but the angle between the electron density associated with the thiazolium and methylaminopyrimidine rings is more acute than that in any of the 26 known three-dimensional structures of nine ThDP-dependent enzymes.

In order to fit the two rings into the observed electron density while maintaining planarity at N-3 (Fig. 4*A*), it is necessary to propose a bond angle of 96° at C-7′ and of 90° at the methylene that links to the diphosphate tail of the cofactor. These unfavorable angles are each about 15° more acute than those observed in other ThDP-dependent enzymes, which average 111° (range 107–115°) and 107° (range 103–112°), respectively. An alternative explanation is that the structure is pyramidal at N-3 (Fig. 4*A*), resulting in acceptable bond angles of 110° and 104°, respectively. At 2.3-Å resolution the electron density is not sufficiently well resolved to discriminate between the two possibilities. However, our preferred model is that with a pyramidal N-3 because there is a reasonable mechanism that could give rise to this structure.

A pyramidal N-3 could arise from an improbable reduction by DTT to the thiazoline (44) or by charge migration from N-3 to S-1 (Fig. 5, ***Ia***). Kluger (27) noted the importance of **Ia** to the probable structure of the carbanion. Although this S^+ form is expected to be less favored than the N^+ form, the difference in stability between the two forms may be small. In the crystal structure of ThDP itself (45), the N^+ form is favored by a factor of 2.16:1 only. Moreover, the Met^{394} backbone carbonyl dipole, 3.9 Å from S-1 but 6.3 Å from N-3, may provide some weak stabilization of the S^+ form. Irrespective of how it is stabilized, we suggest that the structure observed is the **Ia/Ib** resonance hybrid with **Ib** as a significant contributor. However, we cannot rule out C-2 proton dissociation giving the resonating sulfur ylide/carbene (**IIa/IIb**).

In all ThDP-dependent enzymes, the two rings of the cofactor are held in a V conformation by a large hydrophobic residue intruding between them. For example, in yeast AHAS it is Met^{525} that performs this role. The structurally equivalent residue in *K. pneumoniae* ALS is Met^{422}, and the position of this methionine is quite similar in the two enzymes (not shown), with a Cα separation of only 0.64 Å. The position of Met^{422} allows a pyramidal N-3, but it does not force this conformation. Observations on the structure of ALS containing a bound intermediate, to be described below, suggest an explanation for the unusual conformation. This hypothesis will be developed under "Discussion," but it involves formation of the tricyclic form **IIc** (Fig. 5).

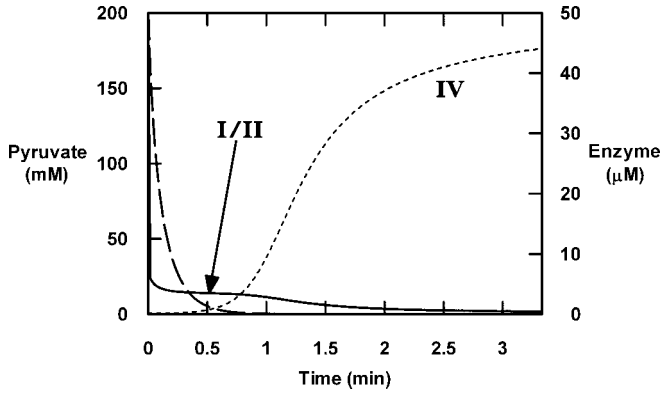

FIG. 6. **Simulation of the time-dependent distribution of enzyme complexes as pyruvate is consumed by ALS.** Complexes **I** and **II** (Fig. 1*A*) were treated as a single species. The rate constants assumed are as follows: **I/II** → **III**, 2.5×10^4 M^{-1} s^{-1}; **III** → **I/II**, 1.0×10^3 s^{-1}; **III** → **IV**, 1.5×10^3 s^{-1}; **IV** → **V**, 7.0×10^5 M^{-1} s^{-1}; **V** → **IV**, 5.0×10^1 s^{-1}; **V** → **I/II**, 5.5×10^2 s^{-1}; and **I/II** → **V**, 1.0×10^5 M^{-1} s^{-1}. This combination of rate constants results in k_{cat} and K_m values of 500 s^{-1} and 34.1 mM, respectively. Initial concentrations of pyruvate and ALS were set at 200 mM and 50 μM, respectively. Simulations were performed with the program Wes (46). The *dashed line* shows pyruvate consumption, and the *solid* and *dotted lines* show the concentrations of **I/II** and **IV**, respectively. When pyruvate consumption exceeds 99% after about 0.7 min, there is a sharp rise in the amount of **IV**, and at 3 min this enzyme form represents about 85% of the total. The percentage of **IV** rises above 98% upon continuing the simulation (not shown) for a further 12 min and eventually reaches 100%.

ALS with a Bound Intermediate

Rationale for the Addition of Pyruvate—Crystals of the enzyme were soaked with pyruvate to convert the enzyme to intermediate **IV** (Fig. 1*A*). The overall reaction catalyzed by ALS is irreversible, and it may not be immediately apparent why addition of pyruvate would cause the accumulation of what is, ostensibly, a transient intermediate. However, when the catalytic cycle of the enzyme (Fig. 1*A*) is dissected, it can be shown that accumulation of this intermediate is not only possible, it is obligatory. Addition of pyruvate initiates the catalytic cycle, which proceeds in a predominantly clockwise direction as illustrated in Fig. 1*A*. In the steady state, **IV** represents a small fraction of the total enzyme present, but as acetolactate accumulates, reversal of the step **I** → **V** becomes possible. Accumulation of acetolactate is accompanied by depletion of pyruvate so **V** → **IV** is increasingly favored. For as long as some pyruvate remains, all enzyme forms will coexist in steady-state equilibrium. However, the pyruvate concentration will be driven to zero eventually by reaction with **II** forming **III,** which is converted irreversibly to **IV**. At the same time, **IV** → **V** becomes impossible because there is no pyruvate remaining. The combination of these processes forces the total active enzyme to collect as **IV**.

To verify this logic, a simulation was performed (Fig. 6) by using the program Wes (46). We do not suggest that the simulation illustrated reproduces quantitatively the time course of the various intermediates, and we did not perform an exact simulation because we do not know the values of the various rate constants. However, no matter what rate constants are assumed, the simulation always terminates with **IV** as the final form. The only escape would be the release of acetaldehyde to produce **I**, a reaction that is not part of the catalytic cycle and is expected to be suppressed by ALS. Even if this reaction does occur slowly, the built-up acetolactate would ensure that **IV** is immediately reformed from **I** via **V**.

Overall Structure of the Protein—Crystals in two different space groups (Table I) were treated with pyruvate to trap the intermediate. The triclinic form has the highest resolution at

TABLE I
Data collection and refinement statistics

	Resting	Intermediate O[a]	Intermediate T[a]
Crystal data			
Unit cell length (Å)	a = 116.8	a = 117.5	a = 86.3
	b = 160.6	b = 160.6	b = 92.8
	c = 129.4	c = 129.5	c = 97.4
Unit cell angle (°)	α = 90.0	α = 90.0	α = 68.0
	β = 90.0	β = 90.0	β = 63.5
	γ = 90.0	γ = 90.0	γ = 67.7
Space group	$C222_1$	$C222_1$	$P1$
Crystal dimensions (mm)	0.2 × 0.05 × 0.05	0.2 × 0.05 × 0.05	0.3 × 0.3 × 0.05
Diffraction data[b]			
Temperature (K)	100	100	100
Resolution range (Å)	100–2.3	100–2.3	100–2.0
Observations [I>0σ(I)]	195,326 (4677)	170,273 (5047)	285040 (17,104)
Unique reflections [I>0σ(I)]	48,069 (2370)	48,466 (3030)	153,254 (11,633)
Completeness	87.5 (43.7)	88.2 (49.3)	93.8 (71.3)
R_{sym}[c]	0.055 (0.113)	0.057 (0.126)	0.030 (0.14)
$\langle I\rangle/\langle\sigma(I)\rangle$	21.5 (5.6)	17.7 (4.5)	29.2 (4.6)
Refinement			
Resolution limits (Å)	100–2.3	100–2.3	100–2.0
Monomers per asymmetric unit	2	2	4
No. atoms per asymmetric unit[d]			
Protein non-H	8204 (24.4)	8256 (25.6)	16,260 (33.1)
ThDP non-H	2 × 26 (21.1)		
ThDP/intermediate non-H		2 × 29 (18.7)	4 × 29 (22.9)
Mg^{2+}	2 (13.9)	2 (12.8)	4 (24.2)
Phosphate non-H	2 × 5 (16.4)	2 × 5 (19.8)	4 × 5 (40.6)
Diethylene glycol non-H	9 × 7 (45.0)	8 × 7 (50.0)	5 × 7 (52.9)
Triethylene glycol non-H			2 × 10 (48.9)
Water molecules	527 (34.1)	612 (36.3)	1335 (42.3)
R_{factor}	0.165	0.162	0.191
R_{free}	0.215	0.214	0.228
Root mean square deviations			
Bond lengths (Å)	0.005	0.005	0.005
Bond angles (°)	1.24	1.23	1.26
Ramachandran plot (%)			
Most favored	91.1	90.6	90.6
Additionally allowed	8.8	9.4	9.3
Generously allowed	0.1	0.0	0.1
Disallowed	0.0	0.0	0.0

[a] Enzyme-intermediate complex, formed by soaking orthorhombic (O) or triclinic (T) crystals with 200 mM pyruvate.
[b] Values in parentheses are statistics for the highest resolution shell, 2.38 to 2.30 Å for the orthorhombic crystals and 2.07 to 2.00 Å for the triclinic crystal.
[c] $R_{sym} = \Sigma|I-\langle I\rangle|/\Sigma\langle I\rangle$, where I is the intensity of an individual measurement of each reflection and $\langle I\rangle$ is the mean intensity of that reflection.
[d] Values in parentheses are average B-factors, in Å^2.

2.0 Å, and the asymmetric unit is a tetramer. For the orthorhombic form, the asymmetric unit contains two monomers and diffracts to 2.3 Å, the same as this form when not soaked with pyruvate. There are only marginal differences between the triclinic and orthorhombic forms, and here we shall focus on the latter when describing the protein structure. When we look in detail at the intermediate, the data from the triclinic form will be used because it has the higher resolution.

Monomer A extends from Pro^6 to His^{554} and contains no internal gaps, whereas monomer B has one additional N-terminal residue and has gaps at Val^{118}–Gln^{120}, Gly^{185}, and Gly^{363}. No side-chain electron density beyond the β-carbon is observed for Lys^{114}, Ser^{184}, Lys^{208}, and Lys^{225} in monomer A and Gln^{117}, Ser^{184}, Gln^{188}, Arg^{350}, Arg^{361}, and Arg^{362} in monomer B. The overall structure of the two monomers is almost identical with an r.m.s.d. of 0.70 Å for 540 Cα atoms. Comparing each monomer with the two of the resting enzyme, the differences are again rather small; of the four possible pairwise comparisons, the highest r.m.s.d. is 0.78 Å for 536 Cα atoms. When the active site regions of the resting and enzyme-intermediate forms are compared, the positions of all amino acid side chains are identical within the resolution of the data.

Structure of the Intermediate—The geometry of ThDP in the intermediate is subtly different from that in the resting enzyme. One major difference is the presence of additional electron density that projects from C-2 (Fig. 4, *B* and *C*), consistent with the presence of the *S*-enantiomer of an hydroxyethyl group attached to the cofactor. A further difference is that the methylaminopyrimidine and thiazolium rings are closer to one another than in the resting enzyme. We investigated a variety of conformational alternatives for the cofactor, but these invariably left unexplained electron density between N-4′ and C-2 (Fig. 4*F*). Even when these two atoms were separated by 2.2 Å only, closer than the sum of their van der Waals radii (2.95 Å), unexplained density remained. Our interpretation is that there is a covalent bond connecting N-4′ and C-2 (Fig. 4*E*).

The resulting tricyclic compound (***IVc***, Fig. 5) is identical to dihydrothiachrome diphosphate except for the extra substituent on C-2. The formation of dihydrothiachrome by cyclization of thiamine in alkaline ethanol was first detailed by Maier and Metzler (47). Oxidation of this compound gives rise to thiochrome (48), the fluorescent derivative that is used widely for estimating thiamine and its derivatives. Later studies have reported the formation of dihydrothiachrome in basic (49) and neutral (50) aqueous solution. It was suggested (51), before the structure of any ThDP-dependent enzyme was known, that the tricyclic form may be catalytically important as a means of protecting ThDP from hydrolysis. Even though the enzyme structures published subsequently have not favored this hypothesis, Zoltewicz and Uray (49) do not rule it out. Similar tricyclic structures may form in other ThDP-dependent enzymes, and in this context we note that the drug omeprazole,

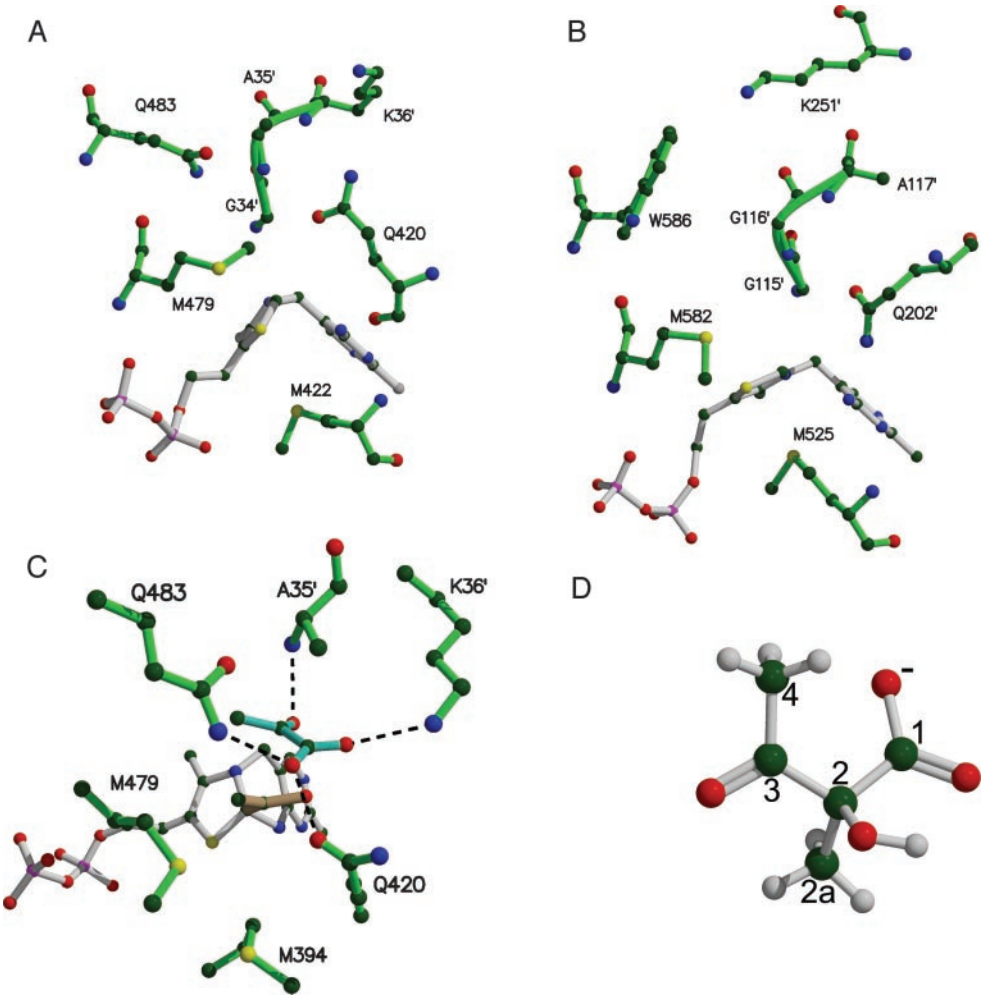

FIG. 7. **The active sites of ALS and AHAS.** *A* shows the active site region of *K. pneumoniae* ALS (resting enzyme), and *B* shows the active site of yeast AHAS viewed in a similar orientation. Residues with and without the *prime symbol* are derived from different monomers. *C*, the active site of ALS is shown with the second molecule of pyruvate modeled in so that it makes favorable contacts and is orientated so that it would yield the *S*-enantiomer of acetolactate (*D*). In this model, the intermediate is represented as the tricyclic carbanion (***IVb***, Fig. 5), and an alternate conformation of Lys^{36} is shown for which the ϵ-amino group forms an ionic interaction with the carboxylate of the second pyruvate.

an analog of the tricyclic form of thiamine, inhibits *Z. mobilis* pyruvate decarboxylase by competing with ThDP (52).

The structure that we propose has not been identified previously as a possible intermediate of a ThDP-dependent enzyme. Indeed, we think that it is more likely to be a non-productive complex (***IVc,*** Fig. 5) formed in a side reaction from the true intermediate (***IVb***, Fig. 5). We suggest that the highly reactive tricyclic intermediate (***IIc,*** Fig. 5) first forms prior to addition of the first pyruvate, and this reacts with the substrate forming **III** that then decarboxylates to give the relatively non-reactive enamine (***IVa***, Fig. 5). Because this is stable, the enzyme can pause midway through the catalytic cycle while releasing CO_2 and admitting the second molecule of pyruvate. The tricyclic α-carbanion (***IVb***, Fig. 5) then forms, ready to react with the second pyruvate. However, occasionally during the prolonged incubation that occurs after the soaked crystals have used up all of the added pyruvate, a small fraction of the accumulated **IVa** flickers into **IVb** and is converted to **IVc**, which is the stable product that we observe. This two-step route (**IVa** $\rightarrow$ **IVb** $\rightarrow$ **IVc**) appears to be the more likely, although we cannot rule out direct conversion of **IVa** to **IVc**.

The conversion of **IVb** to **IVc** involves protonation of Cα of the intermediate and deprotonation of N-4′. Although these could be unconnected events, we suggest that there is an intramolecular proton transfer. The basis of this suggestion is that the hydrogen atom on Cα of **IVc** is in a hydrophobic region with no suitable amino acid side chains or water molecules that might be a proton source. The N-4′ hydrogen atom on the hydrophobic face of **IVb** is well positioned to act as a source of the Cα proton, with a C to N distance of 2.4 Å.

Active Site and a Second Substrate Binding Model

As in AHAS, the active site of ALS is located at a dimer interface, situated at the bottom of a funnel about 15–20 Å from the surface of the protein. The inner face of this funnel is bordered by amino acids from all three domains and from both monomers of the functional dimer. When the active sites of ALS and AHAS are compared (Fig. 7, *A* and *B*), the similarities between the type and orientation of functional groups are apparent. In both enzymes, the C-2 reaction center is flanked on one side by a hydrophobic residue and on the other side by a glutamine. The hydrophobic residues (Met^{479} in ALS and Met^{582} in AHAS) are conserved both in their positions within the active sites as well as in the primary sequences. On the other hand, the glutamine residues (Gln^{420} in ALS and Gln^{202} in AHAS) occupy similar positions in the active sites but are from totally different parts of the proteins; Gln^{420} in ALS is from the γ-domain, and Gln^{202} in AHAS is from α-domain and a different monomer. There is growing recognition (53) that related proteins can have spatially equivalent functional groups in their active sites that occupy different positions in their amino acid sequences.

The second half of the ALS/AHAS catalytic cycle (Fig. 1*A*) involves the combination of the reaction intermediate (**IV**) with the second substrate to yield the bound product complex (**V**) that then releases an acetohydroxy acid. The formation of the product intermediate is stereospecific, and the incoming substrate must be correctly orientated. This might involve an ionic interaction between the carboxylate group and a basic residue in the active site. The only available candidate residues are Lys^{36} in ALS and Lys^{251} in AHAS. As with the Gln^{420}/Gln^{202} pair, the lysine residues are not from corresponding positions in amino acid sequence, but they are found in similar locations within the active sites of the two enzymes. These lysines are highly conserved within the two groups of enzymes, and their side chains are not involved in ionic interactions with other parts of the protein. We suggest that they are involved in binding and orientating the second substrate.

By using the information from the crystal structures and the reaction stereochemistry, a model for the binding of the second substrate in ALS is proposed (Fig. 7*C*). In the description of this model, we will refer to atoms as they are numbered in the acetolactate product (Fig. 7*D*), in which C-3 and C-4 are derived from the first pyruvate, and C-1, C-2, and C-2a are derived from the second pyruvate. We believe that the covalently bound intermediate that reacts with the second substrate is a tricyclic hydroxyethyl carbanion (***IVb***, Fig. 5), and our proposal (Fig. 7*C*) is based on modeling this structure. The intermediate would be planar at C-3 with its methyl group (C-4) interacting with Met^{479} and its hydroxyl group pointing toward the solvent cavity. The *re* face of the intermediate will be buried in a hydrophobic cavity (consisting of the side chains of Met^{394}, Met^{479}, and the β-carbon atom of Gln^{420}) and the *si* face toward the solvent cavity where the second pyruvate is most likely to bind.

The formation of **V** involves the nucleophilic attack of **IVb** on the C-2 atom of the second pyruvate. The product released is acetolactate with a chiral center at C-2. The *S*-enantiomer is required for branched-chain amino acid biosynthesis (54), and we have found by circular dichroism spectroscopy (data not shown) that the products of ALS and AHAS have the same stereochemistry. Thus, in order to produce the correct enantiomer of acetolactate, the second pyruvate must be bound to ALS with its C-2 atom close to the C-3 carbanion of the intermediate, and orientated so that it will produce the *S*-enantiomer of acetolactate.

In our model, the second pyruvate is bound in the active site solvent cavity and with its two carbonyl oxygens displacing two water molecules that are present in the crystal structures of ALS containing the intermediate. The C-2 oxygen forms a hydrogen bond with the backbone nitrogen of Ala^{35}, and the C-2a methyl group points toward Gln^{483}. The residue corresponding to Gln^{483} in AHAS is Trp^{586} (Fig. 7*B*) and has been shown to be involved in second substrate specificity (55). Although AHAS favors 2-ketobutyrate as the second substrate, ALS reacts very poorly with the larger substrate (56). We have tried to model 2-ketobutyrate into the ALS active site, but this results in steric clashes between the larger ethyl group of 2-ketobutyrate and the extended side chain of Gln^{483}. In order to accommodate 2-ketobutyrate, Gln^{483} would have to adopt an alternate conformation in which its side chain moves toward the protein surface and out of the active site. Gln^{483} may play a role in ALS catalysis so this drastic change in its conformation in order to bind to 2-ketobutyrate would prevent reaction from occurring.

The C-1 carbonyl oxygen of the modeled pyruvate is positioned in place of a water molecule that is found between and hydrogen-bonded to the side chains of Gln^{420} and Gln^{483}. The nearest carboxylate oxygen of pyruvate is about 4 Å away from the side chain of Lys^{36}. However, this side chain can be moved easily so that it could form an ionic interaction with the carboxyl group of the second pyruvate, assisting its binding and orientation. Our model positions the second pyruvate with its C-2 atom close to the C-3 carbanion (3.8 Å) and in the right orientation to produce 2*S*-acetolactate. The second substrate may be bound in a similar way in AHAS because the architecture of their active sites is very similar (Fig. 7, *A* and *B*) and they produce acetolactate with the same stereochemistry.

Extraneous Ligands

Each monomer in both orthorhombic forms of the enzyme contains several 7.4 Å long sausage-shaped regions of electron density in the asymmetric unit, one of which in each monomer is in a pocket close to the entrance of the channel leading to the active site. The electron density fits well to diethylene glycol and may represent an immobile segment of a much larger molecule, either the precipitant PEG8000 or the cryoprotectant PEG600. Monomer A of the triclinic form contains two molecules of what appears to be triethylene glycol. In this context we note that other crystal structures contain ligands modeled as triethylene glycol, and Lehtiö *et al.* (57) suggest that they are observing part of a PEG1000 molecule that was used as a precipitant. Four of the diethylene glycol molecules in each orthorhombic monomer form two clusters, each of which may be part of a single PEG molecule. A geometrically plausible ethyl connection can be made between the two molecules in each pair, and there is weak electron density in this region suggestive of such connections.

In all three structures, each monomer contains a tetrahedral island of electron density in an equivalent position, which was modeled as a phosphate ion because the enzyme storage buffer contains 50 mM potassium phosphate. The phosphate ion is located near the C-terminal end of helix $\alpha 15/\eta 10$ at the junction of the β- and γ-domains. In the crystal structures of yeast AHAS (9, 40), a potassium ion is found at the equivalent position. In AHAS, this cation stabilizes the dipole of its interacting helix, and it is unexpected for a phosphate ion to be found at the same location. However, the phosphate ion in ALS is charge-neutralized by three arginine residues (Arg^{259}, Arg^{352}, and Arg^{403}) that surround it. Other ligands include the side chain of Gln^{266} and a water molecule. This phosphate ion may be functionally significant because it is known that ALS is activated by acetate, and this activation is reversed by phosphate and sulfate (58, 59).

DISCUSSION

FAD and the β-Domain—The absence of FAD in ALS and its presence in AHAS could be explained in two ways. The first explanation is that ALS comes from the same evolutionary line as AHAS with both derived from an FAD-dependent pyruvate oxidase-like ancestor; subsequently, ALS has dispensed with the requirement for FAD. Alternatively, ALS may have originated from the same line as the 2-ketoacid decarboxylases that do not contain FAD, such as pyruvate decarboxylase, indolepyruvate decarboxylase, and benzoylformate decarboxylase. This explanation implies that AHAS and ALS are the result of convergence of function with respect to the reaction catalyzed. Phylogenetic analysis of the protein sequences (60) shows that the ALS sequences cluster closely together and are part of a larger group that includes pyruvate oxidase and AHAS. The 2-ketoacid decarboxylases form an entirely separate cluster. These data clearly indicate that ALS comes from the same pyruvate oxidase-like ancestor as AHAS. FAD has a purely structural role in AHAS that has been supplanted in ALS by adjustment of the protein. This has involved a series of amino

acid substitutions and reorientations that fill the channel occupied by FAD in AHAS (Fig. 2, *C* and *D*).

Structures of the enzymes mentioned above have been published (9, 13–18, 40). All have a similar three-domain structure with a core composed of pairs of α- and γ-domains, with the β-domains on the periphery. The active sites are at the junction of the α-domain of one subunit and the γ-domain of its neighbor. Also in this structural family is transketolase with the same three-domain structure but arranged in the sequence γ, α, and β (12).

A clear role for the β-domain has been established in pyruvate oxidase, where it constitutes the major portion of the binding site for FAD (14), a required participant in catalysis. In yeast (but not *Z. mobilis*) pyruvate decarboxylase, an allosteric activator site that binds pyruvate, is in the β-domain (15). We have suggested (40) that the β-domain of yeast AHAS forms part of the binding site for the regulatory subunit of this enzyme. For the other enzymes, the β-domain has no obvious function and appears to serve solely as a scaffolding to support the α- and γ-domains. Thus, the absence of an FAD-binding site in the β-domain of ALS reflects mutations that have occurred after separation from the AHAS evolutionary lineage. Given that pyruvate decarboxylase, benzoylformate decarboxylase, indolepyruvate decarboxylase, and transketolase can construct a perfectly satisfactory β-domain scaffold without FAD, it is no great surprise that ALS can do the same.

If the role of the β-domain in most of these enzymes is solely to hold the α- and γ-domains together, then one might easily imagine related enzymes that have dispensed with the β-domain entirely by developing appropriate interactions between the α- and γ-domains. This appears to be the situation in phosphonopyruvate decarboxylase (61) where the protein sequence corresponding to the β-domain is missing, whereas in sulfopyruvate decarboxylase there are separate subunits that are homologous to the α- and γ-domains, with no equivalent to the β-domain (61). Thus, this entire family of enzymes is constructed around the α- and γ-domains. The β-domain can be involved in regulation (yeast pyruvate decarboxylase and perhaps AHAS), structural integrity (ALS, *Z. mobilis* pyruvate decarboxylase, benzoylformate decarboxylase, indolepyruvate decarboxylase, and transketolase), or not required at all (phosphonopyruvate decarboxylase and sulfopyruvate decarboxylase). Only in pyruvate oxidase does the β-domain have an indispensable role in catalysis.

ThDP—There are published structures of representatives of most major classes of ThDP-dependent enzymes, which show recognizable common themes in the interactions and conformation of ThDP. It is anchored to the protein through a divalent metal ion that ligates to the diphosphate tail and a pair of polar amino acid side chains from the borders of the thiamine-binding motif (41). N-1′ forms a hydrogen bond to a conserved glutamate residue that plays an important role in catalysis (20–24). The cofactor is held in a V conformation by a large hydrophobic residue that projects between the thiazolium and methylaminopyrimidine rings. This forces the 4′-amino group into close proximity with C-2 of the thiazolium ring. ThDP in ALS displays all of these features but differs in one crucial respect. N-3 of the thiazolium ring is pyramidal in our interpretation, whereas in all of the other structures it is trigonal. The protein itself does not appear to force this pyramidal conformation, so what are the forces that bring about this unique structure?

An important clue comes from the structure of ALS with the trapped hydroxyethyl intermediate, where ThDP is in its tricyclic form (29). A similar dihydrothiachrome compound has been documented previously for thiamine in solution (47, 49, 50), but never before has it been observed in an enzyme. Superimposition of ThDP in the resting enzyme with that in the intermediate (Fig. 4*D*) demonstrates that the cofactor atoms are in very similar positions. Therefore, we suggest that the resting enzyme contains both the open and tricyclic (***IIc***, Fig. 5) forms of ThDP in rapid equilibrium. The proportion of the dihydrothiachrome form is small enough that it makes no major contribution to the electron density but large enough to favor maintenance of N-3 in its pyramidal conformation.

We propose that the tricyclic ThDP reacts with pyruvate forming the tricyclic lactyl-ThDP (***III***, Fig. 5). After decarboxylation, the enamine (***IVa***, Fig. 5) is kinetically stabilized against reaction with electrophiles because the forced pyramidal N-3 prevents delocalization of electron density from N-3 to the nucleophilic center at the substrate-derived C-3. The active site can then pause to release CO_2 and admit the second molecule of pyruvate with no risk of diversion into a non-productive product. However, during the extended incubation of crystallization, the proximity of N-4′ allows occasional reaction at C-2 of the thiazolium ring and proton transfer to the substrate-derived C-3 forming **IVc** (Fig. 5), the product that we have found.

An intriguing implication of our favored structure for ThDP and mechanism is that they may explain the unusually high k_{cat} of *K. pneumoniae* ALS. The enforced non-planarity at N-3, which we propose for the reasons described earlier, would result in a structure in which greater positive charge is distributed onto C-2, because delocalization of this charge onto N-3 would not be possible and S-1 would be less able to bear positive charge than N-3, also for the reasons given above. The result should be a more acidic C-2—H bond. After ionization to **IIa/IIb**, cyclization would then produce the nearly localized carbanion **IIc** which should exhibit very high nucleophilic reactivity toward the first pyruvate. By forcing pyramidal geometry at N-3, the enzyme would therefore promote C-2 reactivity and accelerate the steps leading to lactyl-ThDP (***III***, Fig. 5), which are rate-limiting in AHAS (62).

The prevailing evidence (1, 12–19, 26) suggests that the 4′-amino group of ThDP, possibly as an imino group in a tautomer of the methylaminopyrimidine ring, functions as a basic center in C-2 deprotonation. The mechanistic proposal of Fig. 5 can readily accommodate this role. This mechanism is consistent with the structures that we observe and is compatible with the known chemical properties of ThDP and the catalytic properties of ThDP-dependent enzymes. We speculate that in ALS we may be observing forms of the cofactor that are relevant to other ThDP-dependent enzymes. Perhaps the high k_{cat} of ALS favors retention of these unusual, but crucial, conformations. Only the more relaxed structures are observed in other ThDP-dependent enzymes, because they are less able to keep ThDP in its most active state.

Acknowledgments—H.-L. Peng (National Chiao Tung University, Taiwan) and H.-Y. Chang (National Tsing Hua University, Taiwan) provided the original clone used as a source of the *K. pneumoniae* ALS gene. We thank R. Kluger (University of Toronto, Canada), J. V. Schloss (Kuwait University, Kuwait), and F. J. Leeper (University of Cambridge, UK) for useful comments on the nature and significance of the ThDP structures reported here. All misinterpretations are our own. The use of the BioCARS sector was supported by the Australian Synchrotron Research Program, which is funded by the Commonwealth of Australia under the Major National Research Facilities Program. Use of the Advanced Photon Source was supported by the United States Department of Energy, Basic Energy Sciences, Office of Energy Research, under Contract W-31-109-Eng-38. We thank Dr. Keith Brister and Dr. Harry Tong for help with data collection at the Advanced Photon Source.

REFERENCES

1. Duggleby, R. G., and Pang, S. S. (2000) *J. Biochem. Mol. Biol.* **33,** 1–36
2. Gollop, N., Damri, B., Barak, Z., and Chipman, D. M. (1989) *Biochemistry* **28,** 6310–6317
3. Bornemann, S. (2002) *Nat. Prod. Rep.* **19,** 761–772
4. Osborne, A., Thorneley, R. N. F., Abell, C., and Bornemann, S. (2000) *J. Biol. Chem.* **275,** 35825–35830
5. Vargo, D., Pokora, A., Wang, S. W., and Jorns, M. S. (1981) *J. Biol. Chem.* **256,** 6027–6033
6. Wajant, H., and Effenberger, F. (1996) *Biol. Chem. Hoppe-Seyler* **377,** 611–617
7. Dreveny, I., Gruber, K., Glieder, A., Thompson, A., and Kratky, C. (2001) *Structure* **9,** 803–815
8. Chang, Y.-Y., and Cronan, J. E., Jr. (1988) *J. Bacteriol.* **170,** 3937–3945
9. Pang, S. S., Duggleby, R. G., and Guddat, L. W. (2002) *J. Mol. Biol.* **317,** 249–262
10. Störmer, F. C. (1967) *J. Biol. Chem.* **242,** 1756–1759
11. Pang, S. S., Guddat, L. W., and Duggleby, R. G. (2002) *Acta Crystallogr. Sect. D Biol. Crystallogr.* **58,** 1237–1239
12. Lindqvist, Y., Schneider, G., Ermler, U., and Sundström, M. (1992) *EMBO J.* **11,** 2373–2379
13. Dyda, F., Furey, W., Swaminathan, S., Sax, M., Farrenkopf, B., and Jordan, F. (1993) *Biochemistry* **32,** 6165–6170
14. Muller, Y. A., Schumacher, G., Rudolph, R., and Schulz, G. E. (1994) *J. Mol. Biol.* **237,** 315–335
15. Arjunan, P., Umland, T., Dyda, F., Swaminathan, S., Furey, W., Sax, M., Farrenkopf, B., Gao, Y., Zhang, D., and Jordan, F. (1996) *J. Mol. Biol.* **256,** 590–600
16. Dobritzsch, D., König, S., Schneider, G., and Lu, G. (1998) *J. Biol. Chem.* **273,** 20196–20204
17. Hasson, M. S., Muscate, A., McLeish, M. J., Polovnikova, L. S., Gerlt, J. A., Kenyon, G. L., Petsko, G. A., and Ringe, D. (1998) *Biochemistry* **37,** 9918–9930
18. Schutz, A., Sandalova, T., Ricagno, S., Hubner, G., Konig, S., and Schneider, G. (2003) *Eur. J. Biochem.* **270,** 2312–2321
19. Schellenberger, A., Hübner, G., and Neef, H. (1997) *Methods Enzymol.* **279,** 131–146
20. Wikner, C., Meshalkina, L., Nilsson, U., Nikkola, M., Lindqvist, Y., Sundström, M., and Schneider, G. (1994) *J. Biol. Chem.* **269,** 32144–32150
21. Candy, J. M., Koga, J., Nixon, P. F., and Duggleby, R. G. (1996) *Biochem. J.* **315,** 745–751
22. Killenberg-Jabs, M., König, S., Eberhardt, I., Hohmann, S., and Hübner, G. (1997) *Biochemistry* **36,** 1900–1905
23. Fang, R., Nixon, P. F., and Duggleby, R. G. (1998) *FEBS Lett.* **437,** 273–277
24. Bar-Ilan, A., Balan, V., Tittmann, K., Golbik, R., Vyazmensky, M., Hübner, G., Barak, Z., and Chipman, D. M. (2001) *Biochemistry* **40,** 11946–11954
25. Hill, C. M., Pang, S. S., and Duggleby, R. G. (1997) *Biochem. J.* **327,** 891–898
26. Kern, D., Kern, G., Neef, H., Tittmann, K., Killenberg-Jabs, M., Wikner, C., Schneider, G., and Hübner, G. (1997) *Science* **275,** 67–70
27. Kluger, R. (1987) *Chem. Rev.* **87,** 863–876
28. Chabrière, E., Vernede, X., Guigliarelli, B., Charon, M. H., Hatchikian, E. C., and Fontecilla-Camps, J. C. (2001) *Science* **294,** 2559–2563
29. Fiedler, E., Thorell, S., Sandalova, T., Golbik, R., König, S., and Schneider, G. (2002) *Proc. Natl. Acad. Sci. U. S. A.* **99,** 591–595
30. Otwinowski, Z., and Minor, W. (1997) *Methods Enzymol.* **276,** 307–326
31. Navaza, J. (1994) *Acta Crystallogr. Sect. A Biol. Crystallogr.* **50,** 157–163
32. Jones, T. A., Zou, J. Y., Cowan, S. W., and Kjeldgaard, M. (1991) *Acta Crystallogr. Sect. A* **47,** 110–119
33. Brünger, A. T., Adams, P. D., Clore, G. M., DeLano, W. L., Gros, P., Grosse-Kunstleve, R. W., Jiang, J.-S., Kuszewski, J., Nilges, M., Pannu, N. S., Read, R. J., Rice, L. M., Simonson, T., and Warren, G. L. (1988) *Acta Crystallogr. Sect. D Biol. Crystallogr.* **54,** 905–921
34. Evans, S. V. (1993) *J. Mol. Graphics* **11,** 134–138
35. Kraulis, P. J. (1991) *J. Appl. Crystallogr.* **24,** 946–950
36. Merritt, E. A., and Bacon, D. J. (1997) *Methods Enzymol.* **277,** 505–524
37. Gouet, P., Courcelle, E., Stuart, D. I., and Metoz, F. (1999) *Bioinformatics* **15,** 305–308
38. Peng, H.-L., Wang, P.-Y., Wu, C.-M., Hwang, D.-C., and Chang, H.-Y. (1992) *Gene* (*Amst.*) **117,** 125–130
39. Huseby, N.-E., Christensen, T. B., Olsen, B. R., and Størmer, F. C. (1971) *Eur. J. Biochem.* (*Tokyo*) **20,** 209–214
40. Pang, S. S., Guddat, L. W., and Duggleby, R. G. (2003) *J. Biol. Chem.* **278,** 7639–7644
41. Hawkins, C. F., Borges, A., and Perham, R. N. (1989) *FEBS Lett.* **255,** 77–82
42. Candy, J. M., and Duggleby, R. G. (1998) *Biochim. Biophys. Acta* **1385,** 323–338
43. Candy, J. M., and Duggleby, R. G. (1994) *Biochem. J.* **300,** 7–13
44. Zoltewicz, J. A., Dill, C. D., and Abboud, K. A. (1997) *J. Org. Chem.* **62,** 6760–6766
45. Pletcher, J., and Sax, M. (1972) *J. Am. Chem. Soc.* **94,** 3998–4005
46. García-Sevilla, F., Garrido-del Solo, C., Duggleby, R. G., García-Cánovas, F., Peyró, R., and Varón, R. (2000) *Biosystems* **54,** 151–164
47. Maier, G. D., and Metzler, D. E. (1957) *J. Am. Chem. Soc.* **79,** 4386–4391
48. Barger, G., Bergel, F., and Todd, A. R. (1935) *Chem. Ber.* **68,** 2257–2262
49. Zoltewicz, J. A., and Uray, G. (1994) *Bioorg. Chem.* **22,** 1–28
50. Washabaugh, M. W., Yang, C. C., Hollenbach, A. D., and Chen, P. (1993) *Bioorg. Chem.* **21,** 170–191
51. Doughty, M. B., and Lawrence, D. S. (1985) *J. Chem. Soc. Chem. Commun.* 454–455
52. Nixon, P. F., Diefenbach, R. J., and Duggleby, R. G. (1992) *Biochem. Pharmacol.* **44,** 177–179
53. Todd, A. E., Orengo, C. A., and Thornton, J. M. (2002) *Trends Biochem. Sci.* **27,** 419–426
54. Sylvester, S. R., and Stevens, C. M. (1979) *Biochemistry* **18,** 4529–4531
55. Ibdah, M., Bar-Ilan, A., Livnah, O., Schloss, J. V., Barak, Z., and Chipman, D. M. (1996) *Biochemistry* **35,** 16282–16291
56. Huseby, N.-E., and Størmer, F. C. (1971) *Eur. J. Biochem.* **20,** 215–217
57. Lehtiö, L., Leppänen, V.-M., Kozarich, J. W., and Goldman, A. (2002) *Acta Crystallogr. Sect. D Biol. Crystallogr.* **58,** 2209–2212
58. Størmer, F. C. (1968) *J. Biol. Chem.* **243,** 3735–3739
59. Holtzclaw, W. D., and Chapman, L. F. (1975) *J. Bacteriol.* **121,** 917–922
60. Bowen, T. L., Union, J., Tumbula, D. L., and Whitman, W. B. (1997) *Gene* (*Amst.*) **188,** 77–84
61. Graupner, M., Xu, H., and White, R. H. (2000) *J. Bacteriol.* **182,** 4862–4867
62. Tittmann, K., Golbik, R., Uhlemann, K., Khailova, L., Schneider, G., Patel, M., Jordan, F., Chipman, D. M., Duggleby, R. G., and Hübner, G. (2003) *Biochemistry* **42,** 7885–7891